



HAL
open science

Transport properties of the Callovo-Oxfordian clay rock under partially saturated conditions

D. Jougnot, A. Revil, N. Lu, A. Wayllace

► **To cite this version:**

D. Jougnot, A. Revil, N. Lu, A. Wayllace. Transport properties of the Callovo-Oxfordian clay rock under partially saturated conditions. *Water Resources Research*, 2010, 46, pp.08514. 10.1029/2009WR008552 . insu-00565207

HAL Id: insu-00565207

<https://insu.hal.science/insu-00565207>

Submitted on 11 Mar 2021

HAL is a multi-disciplinary open access archive for the deposit and dissemination of scientific research documents, whether they are published or not. The documents may come from teaching and research institutions in France or abroad, or from public or private research centers.

L'archive ouverte pluridisciplinaire **HAL**, est destinée au dépôt et à la diffusion de documents scientifiques de niveau recherche, publiés ou non, émanant des établissements d'enseignement et de recherche français ou étrangers, des laboratoires publics ou privés.

Transport properties of the Callovo-Oxfordian clay rock under partially saturated conditions

D. Jougnot,^{1,2,3,4} A. Revil,^{2,3} N. Lu,⁵ and A. Wayllace⁵

Received 23 August 2009; revised 17 February 2010; accepted 26 February 2010; published 6 August 2010.

[1] A series of experiments were performed to characterize the permeability, the specific storage, the capillary pressure, the streaming potential coupling coefficient, and the electrical conductivity of a very low permeability Callovo-Oxfordian clay rock at different water saturations. The Callovo-Oxfordian formation is presently investigated as a potential host to store nuclear wastes because of its very low permeability (typically 10 nd at saturation) and high specific surface area. We first present the constitutive transport equations including an electrokinetic cross-coupling term in the generalized Darcy and Ohm constitutive equations. Then we present new experimental results using measurements of transient weight losses of samples submitted to a change in the relative humidity imposed by an automated humidity system in a hermetic chamber. These experiments are interpreted with a 1-D analytical model of the coupled hydromechanical and transport equations. The hydromechanical transport properties (relative permeability and specific storage) of this clay rock are investigated in the relative saturation range from 0.23 to 0.70. We demonstrate that below 30% in relative humidity, the flux of the vapor phase with respect to the flux of the liquid water phase cannot be neglected. The relative apparent permeability can be described by a simple power law relationship with the saturation. In addition, we measure the electrical conductivity and the streaming potential coupling coefficient at various saturations. The electrical conductivity is described by a model accounting for electrical double-layer contributions to surface conductivity. The measurement of the streaming potential coupling coefficient agrees with a power law model for the coupling coefficient versus the relative water saturation. A relationship between the exponent used to characterize the relative permeability and the second Archie's exponent used to describe the dependence of the electrical conductivity of the material with respect to the saturation is discussed.

Citation: Jougnot, D., A. Revil, N. Lu, and A. Wayllace (2010), Transport properties of the Callovo-Oxfordian clay rock under partially saturated conditions, *Water Resour. Res.*, 46, W08514, doi:10.1029/2009WR008552.

1. Introduction

[2] Argillaceous formations are considered to be potential hosts for nuclear wastes owing to their extremely low intrinsic permeability [e.g., *Gautschi*, 2001; *Croisé et al.*, 2004; *Escoffier et al.*, 2005]. In France, the Radioactive Waste Management Agency (ANDRA, Agence Nationale pour la Gestion des Déchets Radioactifs) is studying the Callovo-Oxfordian (150 Ma) clay rocks formation for an underground (500 m deep) research laboratory in the eastern part of the Paris Basin. During the construction and the future exploitation phase of the waste disposal, the rock mass will be

submitted to various thermohydromechanical stresses. The rock, initially saturated, will partially desaturate owing to the ventilation of the galleries. So it is very important to understand the transport properties in these formations in both saturated and unsaturated conditions including damage related to both desiccation and stress release and healing/sealing effects.

[3] Another important domain for which the knowledge of the hydromechanical properties of low-permeability clay-rich formations acting as seals is important concerns the storage of CO₂ or methane in sedimentary rocks. Indeed, shale and clay rocks can be used as capillary seals to prevent the upward migration, by buoyancy, of a CO₂ plume. However, the modeling of the migration of such a plume requires a description of the transport properties of the clay-rich materials as a function of the saturation of the different fluid phases [*Revil et al.*, 1998].

[4] Very few works have attempted to determine the hydromechanical properties of very low permeability clay rocks under unsaturated conditions because such measurements are very challenging. Recently, *Vales et al.* [2004] and *Giraud et al.* [2007, 2009] used the hydromechanical equations developed by *Coussy* [2004] to show that it is

¹ANDRA, Châtenay-Malabry, France.

²LGIT, UMR 5559, Equipe Volcan, Université de Savoie, CNRS, Le-Bourget-du-Lac, France.

³Department of Geophysics, Colorado School of Mines, Golden, Colorado, USA.

⁴Now at Institute of Geophysics, University of Lausanne, Lausanne, Switzerland.

⁵Division of Engineering, Colorado School of Mines, Golden, Colorado, USA.

possible to determine the relative permeability and the specific storage at near-saturation conditions using measurements of transient weight losses of samples submitted to a change in the relative humidity imposed by an automated humidity system in a hermetic chamber. However, their measurements were restricted to high saturations (for initial relative saturation greater than 0.77). In addition, very few measurements were performed to fully characterize the hydromechanical properties of the Callovo-Oxfordian clay rock in a wide range of saturations (see *Pham [2006]* and *Pham et al. [2007]* for discussions). These measurements are challenging because the amount of fluids that are exchanged by a core sample and the fluid reservoirs are extremely small and therefore very difficult to measure accurately. Therefore, the development of specific methods is required in this case.

[5] In the present paper, we propose a new set of experiments to characterize the Callovo-Oxfordian clay-rock material and especially its hydraulic diffusivity and the capillary pressure curve at different water saturations including very low saturations. The rationale to include in our modeling the behavior of the streaming potential coupling coefficient and electrical conductivity in the generalized Darcy and Ohm equations is that these properties could be important in remotely imaging the state of saturation and pore liquid water flow of these materials using geophysical methods like induced polarization and self-potential [e.g., *Revil and Pezard, 1998; Linde et al., 2007; Crespy et al., 2008; Jougnot et al., 2010*].

2. Background

2.1. Constitutive Transport Equations

[6] We discuss below the fundamental constitutive equations of transport in a linear poroelastic material with very low permeability under unsaturated conditions. The surface of the clay minerals is charged, and this charge is counterbalanced by a charge of opposite sign in the water phase. This characteristic is responsible for two features with respect to previously developed theories. The first feature is the existence of an osmotic pressure term in the fluid pressure of the liquid water phase (recently investigated by *Jougnot et al. [2009]*). The second feature is a cross-coupling term in the constitutive equations for the Darcy velocity of the liquid water phase and the total current density, which represents the flux of electrical charges carried by the flow of the liquid water per unit surface area of the porous material and per unit time. The description of this model has been established with keeping in mind that its specific application to the Callovo-Oxfordian clay rock will be investigated in the following sections.

[7] We use below the subscripts w for the wetting phase (liquid vapor) and n for the nonwetting (dry air, subscript a , mixed with water vapor, subscript v) phase. This distinction is made because the flow of water may occur in principle both as the flow of a liquid plus the transport of vapor by diffusion and advection. We define s_w and s_n as the saturation of the wetting and nonwetting phases, respectively (the saturation condition is expressed as $s_w + s_n = 1$). We further define $\theta_w = s_w\phi$, $\theta_a = s_a\phi$, and $\theta_v = s_v\phi$ the fluid contents of the wetting phase and the two nonwetting phases, respectively, and ϕ stands for the connected porosity of the porous

medium. In addition, we have $s_a = s_v = s_n = (1 - s_w)$. This means that dry air and the water vapor mixes together because they are fully miscible phases (ideal gases). They occupy therefore the same volume fraction of the pore space.

[8] We denote

$$\bar{\mathbf{w}}_w = s_w\phi(\bar{\mathbf{u}}_w - \bar{\mathbf{u}}_s), \quad (1)$$

$$\bar{\mathbf{w}}_n = s_n\phi(\bar{\mathbf{u}}_n - \bar{\mathbf{u}}_s), \quad (2)$$

as the relative displacement vector of the wetting phase relative to the solid phase and the relative displacement vector of the nonwetting phase relative to the solid phase, respectively. The horizontal bar means that these parameters are averaged over the considered phase.

[9] The following assumptions are made throughout the paper: (1) The wetting and nonwetting phases are considered macroscopically inviscid. (2) Temperature gradients and gravitational effects are neglected. (3) Porosity at the scale of a representative elementary volume is considered to change with the stress and the pressures of the fluid phases [*de la Cruz et al., 1993*]. (4) The pore fluids do not bear any shear stresses and the wetting and nonwetting fluid phases are considered to be Newtonian fluids. (5) The water is always in thermodynamic equilibrium with its vapor phase. (6) The liquid water phase has an excess of electrical charges to compensate the surface charge of the minerals that includes the isomorphic substitutions in the crystalline framework, the surface charge at the edge of the clay minerals, and the charge located in the Stern layer (see *Leroy et al. [2007]* for a detailed investigation of the charges onto the various crystalline planes of clay minerals). (7) We consider that the two fluid phases (wetting and nonwetting) are continuous at the scale of a representative elementary volume of the porous body.

[10] We denote

$$\bar{p}_c = \bar{p}_n - \bar{p}_w, \quad (3)$$

as the capillary pressure (expressed in Pa), which depends both on the saturation of the wetting phase and on the history of saturation/desaturation of the porous material, where \bar{p}_n is the phase average of the pressure of the nonwetting phase and \bar{p}_w is the phase average of the fluid pressure in the wetting phase including an osmotic contribution as discussed in detail by *Jougnot et al. [2009]*. For the Callovo-Oxfordian clay rock, we can use the capillary pressure-saturation model proposed by *Vauclin et al. [1979]*:

$$s_w(p_c) = \frac{a_{v,v}}{a_{v,v} + \left(\frac{\bar{p}_c}{\rho_w g}\right)^{b_{v,v}}}. \quad (4)$$

In equation (4), $a_{v,v}$ is a coefficient expressed in meters, $b_{v,v}$ is a dimensionless exponent close to unity, ρ_w is the mass density of liquid water (in kg m^{-3}), and $g = 9.81 \text{ m s}^{-2}$ is the acceleration of the gravity. Some values of $a_{v,v}$ and $b_{v,v}$ found in the literature for the Callovo-Oxfordian clay rock are given in Table 1. We also have $\bar{p}_n = \bar{p}_a + \bar{p}_v$ where \bar{p}_a is the pressure of dry air and \bar{p}_v is the pressure of the water vapor. Using

Table 1. Values of Some Petrophysical Parameters of the Callovo-Oxfordian Clay Rock Determined From Previous Literature Data

Parameter	Value and Uncertainty
a_w	50 ± 25^a
b_w	1.6 ± 0.6^a
α	$0.6^b, 0.75^c$
Log k	-20.0 ± 1.5^d
K	$4.0 \times 10^9 \text{ Pa}^e$
G	$2.4 \times 10^9 \text{ Pa}^f$
a_{vv}	$(10 \pm 6) \times 10^3 \text{ m}^g$
b_{vv}	1.05 ± 0.03^g

^aFrom *Homand et al.* [2004] (drying experiment).

^bBiot coefficient. Value from *Pham* [2006].

^cBiot coefficient. Mean value from *Homand et al.* [2004] and *Giraud et al.* [2009].

^dSaturated apparent permeability (in m^2). Value from *Homand et al.* [2004].

^eDrained bulk modulus. Value from *Homand et al.* [2004].

^fShear modulus of the frame. Value from *Homand et al.* [2004].

^gCapillary pressure curve coefficients. Value from *Giraud et al.* [2009].

this relationship, the dry air pressure can be expressed in terms of the pressure of the nonwetting phase \bar{p}_n and the pressure of the vapor \bar{p}_v phase by $\bar{p}_a = \bar{p}_n - \bar{p}_v$; that is,

$$\bar{p}_v = \bar{p}_v^0 \exp \left[\frac{M_v}{\rho_w R T} (\bar{p}_w - \bar{p}_w^0) \right], \quad (5)$$

$$\bar{p}_v^0 = \bar{p}_v^{\text{sat}}(T) = 10^{f(T)}, \quad (6)$$

$$f(T) = a + (T - T_0)[b + c(T - T_0)]^{-1}, \quad (7)$$

where the index “0” refers to a saturated reference state ($p_c = 0, \bar{p}_w = \bar{p}_n^0 = p_{\text{atm}}$), $T_0 = 273.5^\circ\text{K}$, T is the temperature in Kelvin, $a = 2.7858$ (dimensionless), $b = 31.559 \text{ K}$, $c = 0.1354$ (dimensionless), M_v is the molar mass of vapor (in kg Mol^{-1}), R is the universal gas constant (being $8.31 \text{ J K}^{-1} \text{ Mol}^{-1}$), and \bar{p}_v^0 is the vapor pressure (in Pa) in a water vapor saturated air ($\bar{p}_w = \bar{p}_n^0 = p_{\text{atm}}$). The relative humidity (dimensionless) is obtained by

$$h_r = \frac{\bar{p}_v}{\bar{p}_v^0} = \exp \left[\frac{M_v}{\rho_w R T} (\bar{p}_w - \bar{p}_w^0) \right]. \quad (8)$$

In unsaturated soil mechanics, the suction $\Psi = -p_c$ (in Pa) (or $\Psi = -p_c/\rho_w g$, expressed in m) can be related to the relative humidity h_r by the Kelvin equation [e.g., *Sposito*, 1981]:

$$\Psi = -\frac{RT\rho_w}{M_v} \ln(h_r). \quad (9)$$

[11] We will neglect the viscous drag between the wetting and the nonwetting fluid phases. This assumption is widely accepted in the literature (see *Lo et al.* [2002] for a discussion). In addition, we assume that the material is isotropic and therefore the permeability tensor is described by

$k \mathbf{I}_3$ where k is the isotropic permeability and \mathbf{I}_3 is the 3×3 identity matrix. In the following, we use the constitutive equations of transport discussed by *Revil et al.* [2007] and *Linde et al.* [2007], adding a dispersion-diffusion term to characterize the transport of the vapor and dry air phases through the porous material. The constitutive equations for the flux of the water and vapor phases can be found in the work of *Gawin et al.* [1995]. Adding the cross-coupling term with the current density [*Revil*, 2007], we obtain the following expressions for the volumetric fluxes of the liquid water, water vapor phase, and electrical charges:

$$\dot{\mathbf{w}}_w = -\frac{k_w^r k}{\eta_w} \nabla \bar{p}_w - \frac{k_w^r k}{\eta_w} \left(\frac{\bar{Q}_V}{s_w} \right) \nabla \varphi, \quad (10)$$

$$\dot{\mathbf{w}}_v = -\frac{k_n^r k}{\eta_n} \nabla \bar{p}_n - \mathbf{D} \cdot \nabla \ln C_v, \quad (11)$$

$$\mathbf{j} = -\boldsymbol{\sigma} \cdot \nabla \psi + \left(\frac{\bar{Q}_V}{s_w} \right) \dot{\mathbf{w}}_w, \quad (12)$$

where $C_v = \bar{p}_v/\bar{p}_n$ is the molar concentration of vapor in the nonwetting phase, \bar{Q}_V is the excess of electrical charge of the diffuse layer per unit pore volume at saturation [see *Revil et al.*, 2005; *Jougnot et al.*, 2009], \mathbf{j} is the total current density (in A m^{-2}) (flux of electrical charges per unit surface area and per unit time), $\boldsymbol{\sigma}$ (in S m^{-1}) is a second-order symmetric conductivity tensor of the clay rock (with elements depending on the water saturation), k_w^r is the relative permeability for the water phase (dimensionless), k_n^r is the relative permeability of the nonwetting phase (dimensionless), η_n and η_w are the dynamic viscosities of the nonwetting phase and liquid water phase, respectively (in Pa s), and $\mathbf{E} = -\nabla \varphi$ is the electrical field (in V m^{-1}) (therefore $\nabla \times \mathbf{E} = 0$ is satisfied in the low-frequency limit of the Maxwell equations). In the absence of external electrical field source, φ (in V) is the streaming (macroscopic) potential (in V). In the following, we will assume that anisotropy of the clay rock is not too severe so the conductivity tensor can be replaced by a scalar electrical conductivity.

[12] The positive-definite second-order symmetric tensor \mathbf{D} ($\text{m}^2 \text{ s}^{-1}$) in equation (11) is the effective hydrodynamic diffusion-dispersion tensor in the gas phase. Assuming a Fickian model, it is given by

$$\mathbf{D} = \left[D_m + \alpha_T \frac{\dot{\mathbf{w}}_n}{(s_n \phi)} \right] \mathbf{I}_3 + \frac{\alpha_L - \alpha_T}{(s_n \phi)^2} \frac{\dot{\mathbf{w}}_n}{\dot{\mathbf{w}}_n} \otimes \dot{\mathbf{w}}_n, \quad (13)$$

$$D_m = \frac{s_n D_v}{F}, \quad (14)$$

$$D_v = 2.17 \cdot 10^{-5} \frac{P_{\text{atm}}}{\bar{p}_n} \left(\frac{T}{T_0} \right)^{1.88}, \quad (15)$$

where D_m is the molecular diffusion coefficient of the vapor phase in dry air through the porous material at atmospheric pressure (in $\text{m}^2 \text{ s}^{-1}$), $(\mathbf{a} \otimes \mathbf{b})_{ij} = a_i b_j$ denotes the outer product between vectors \mathbf{a} and \mathbf{b} , α_L and α_T are the longitudinal and transverse dispersivities (in m), respectively, F is the elec-

Table 2. Callovo-Oxfordian Pore Water Composition

THERMOAR Model [Gaucher et al., 2006]		Simplified Solute Composition ^a (Only Charged Species)	
Species	C_i (mol L ⁻¹)	Species	C_i (mol L ⁻¹)
Na	32×10^{-3}	Na ⁺	31.5×10^{-3}
K	7×10^{-3}	K ⁺	6.5×10^{-3}
Ca	15×10^{-3}	Ca ²⁺	9.5×10^{-3}
Mg	14×10^{-3}	Mg ²⁺	8.1×10^{-3}
Cl	30×10^{-3}	Cl ⁻	30×10^{-3}
S(+6)	34×10^{-3}	SO ₄ ²⁻	21×10^{-3}
pH	7.3	-	-
pCO ₂	-2.51	HCO ₃ ⁻	1.2×10^{-3}

^aFrom PHREEQC2; see Leroy et al. [2007].

trical formation factor, which is related to porosity through Archie's law,

$$F = \phi^{-m} \quad (16)$$

[Archie, 1942], m (dimensionless) is called the cementation exponent, p_{atm} is the atmospheric pressure, T is the temperature expressed in K, and $T_0 = 273$ K. This model was developed by de Vries and Kruger [1966] and de Vries [1987] from the kinetic theory of gas and is valid for $273 \text{ K} < T < 373 \text{ K}$. The inverse of the formation factor is the mobile or effective porosity of the porous material [Revil et al., 2003]. Equation (10) describes a generalized constitutive Darcy's equation for the flux of the liquid water phase. The last term corresponds to the electroosmosis contribution associated with the electrical field \mathbf{E} . In absence of an external electrical field, this contribution can be safely ignored.

[13] Finally, equation (13) corresponds to a generalized Ohm's law including the conduction term $-\sigma \nabla \psi$ (classical Ohm's law) plus an advective transport term $(\bar{Q}_V/s_w)\bar{\mathbf{w}}_w$ (the so-called streaming current density; see, for instance, Revil et al. [2007] and Crespy et al. [2008] and references therein). The advective term corresponds to the advective transport of the excess of electrical charges contained in the liquid water phase because of the existence of the electrical double layer at the solid-liquid water interface and a net flux of water with respect to the solid phase. In low-permeability materials, we will further assume that hydrodynamic dispersion can be neglected with respect to diffusion because of the very low permeability of the materials considered in the present work. Therefore, we consider that

$$\mathbf{D} \approx D_m \mathbf{I}_3. \quad (17)$$

In porous materials with clay minerals, electrical conductivity has two contributions. One is associated with the pore water and the second with the electrical double layer coating the surface of the pores [Revil et al., 2002]. For a clay rock, the dependence of the electrical conductivity with the saturation of the water phase can be written as [Revil et al., 2007]

$$\sigma(s_w) = \frac{1}{F} [s_e^n \bar{\sigma}_w + (F - 1)\sigma_S], \quad (18)$$

where $s_e = (s_w - s_w^c)/(1 - s_w^c)$ is the effective saturation, F is the electrical formation factor defined above, n is the second

Archie exponents (n is also called the saturation index), s_w^c is a percolation threshold for the water film connectivity in the second Archie's law, $\bar{\sigma}_w$ (in S m⁻¹) is the pore fluid electrical conductivity (including the disturbances associated with the diffuse layer; see Revil et al. [2006]), and σ_S (in S m⁻¹) represents the electrical conductivity due to electromigration in the Stern layer. This contribution is frequency dependent [Leroy et al., 2008]. Leroy et al. [2008] and recently Leroy and Revil [2009] showed that when a pure DC current is applied, there is no contribution from the Stern layer to the overall electrical conductivity. However, the measurements presented below are performed at 10 Hz, a frequency for which there is contribution from the Stern layer to the overall electrical conductivity of the material as discussed by Leroy and Revil [2009] [see also Revil et al., 2002].

[14] The pore fluid conductivity $\bar{\sigma}_w$ will be calculated below in section 4.3 from the model developed by Leroy et al. [2007]. The complexity arises because the composition of the pore water of the clay rock is distinct from the composition of an ionic reservoir in contact and in equilibrium with the clay materials. This difference is due to the influence of the Coulombic potential of the electrical double layer in the pore space of the material upon the concentrations in anions and cations. The model developed by Leroy et al. [2007] uses a generalized Donnan equilibrium model with a mean (microscopic) electrical potential in the pore water, φ_m (in V). The chemistry of the pore water is computed using the THERMOAR model proposed by Gaucher et al. [2006] (see Table 2 and for more details, see Jougnot et al. [2009]).

[15] The streaming potential is the electrical potential associated with the flow of the pore water. This electrical potential can be used as a powerful nonintrusive method to monitor the flow of the groundwater as shown recently by various studies at different scales, from the laboratory to pumping test experiments in the field [Crespy et al., 2008; Revil et al., 2008; Jardani et al., 2009; Malama et al., 2009]. In the present case, a simple first-order approximation of the electrical field between two electrodes along a cylindrical core sample is employed $(\nabla \varphi)_{\mathbf{j}=0} \approx (\bar{Q}_V/s_w)\bar{\mathbf{w}}_w$ [Linde et al., 2007] indicating that the electrical potential is sensitive to the flow of the liquid water phase only.

[16] In addition to the previous equations, a complete theory should specify the mechanical constitutive and continuity equations for a linear poroelastic body saturated by two fluid phases, the wetting phase (liquid water) and the nonwetting phase formed by a mix between dry air and water vapor. These equations can be found in the work of Homand et al. [2004] for instance and just need to be modified to account for the osmotic pressure in the phase average of the pressure of the wetting (liquid water) phase.

2.2. 1-D Approximation of the Flow Problem

[17] In the following, we consider a cylindrical core sample submitted to different atmospheric relative humidities (see Figures 1–3; see further description in section 3). The bottom and sides of the core samples are impermeable. Therefore the flow is uniaxial (1-D, along the axis of the cylinder as shown in Figure 3). A complete analysis of the 1-D hydromechanical problem is discussed in Appendix A. Such a simplified 1-D approximation of the hydromechanical problem has been developed by Olchitzky [2002] and Homand et al. [2004]. This approximation is based on a

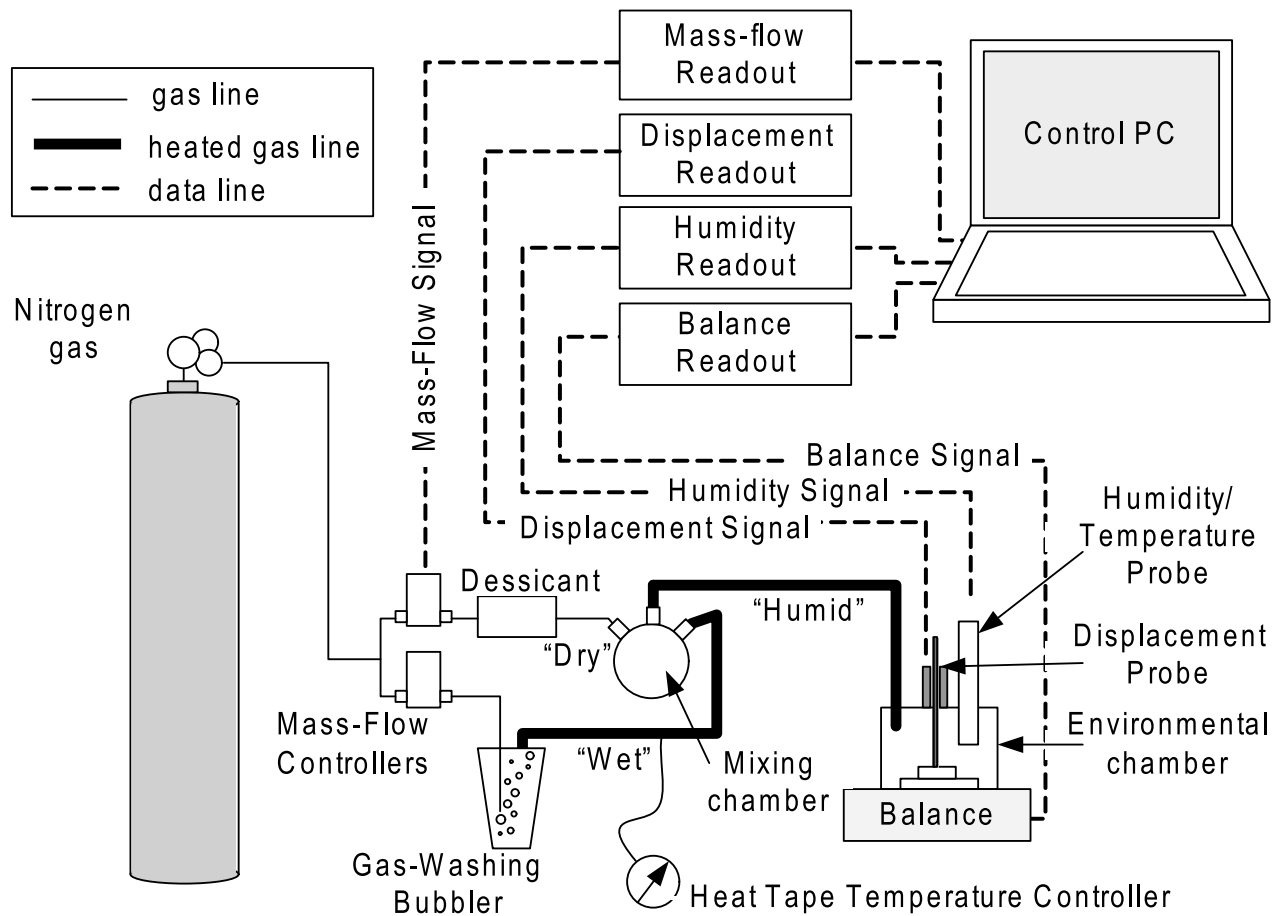


Figure 1. The automated humidity system general layout (modified from *Likos and Lu* [2003]).

linearization of the water saturation–capillary pressure curve using a first-order Taylor series expansion,

$$s_w(\bar{p}_c) = s_w^i + \left(\frac{\partial s_w}{\partial \bar{p}_c} \right)_i (\bar{p}_c - \bar{p}_c^i), \quad (19)$$

$$\left(\frac{\partial s_w}{\partial \bar{p}_c} \right)_i \approx \frac{-a_{vv} / \rho_w g}{\left[a_{vv} + (\bar{p}_c^i / \rho_w g)^{b_{vv}} \right]}, \quad (20)$$

where the superscript i stands for the initial condition during a small change in the saturation of the water phase. Equation (19) is only valid for small variations around the initial capillary pressure value. Using this approximation, *Olchitzky* [2002] and *Homand et al.* [2004] obtained a linearized solution to the hydromechanical problem in unsaturated conditions. The assumptions of this model are the following.

[18] 1. During a small change of the water saturation, all the hydromechanical moduli are constant and equal to their values in the initial saturation state (denoted by the subscript i).

[19] 2. The pressure of the nonwetting phase remains constant in the porous material and is equal to the atmospheric pressure. Therefore the convective term in the flux of the nonwetting phase is neglected.

[20] 3. We compare in Appendix A the vapor transport and liquid water flow terms. Figure 4 shows that the dif-

fusion of the water vapor can be neglected above a relative humidity of 30% and is incorporated into an apparent permeability below this critical value (see a complete derivation in Appendix A). However, the critical value of 30% relative humidity is unusually low for subsurface porous media.

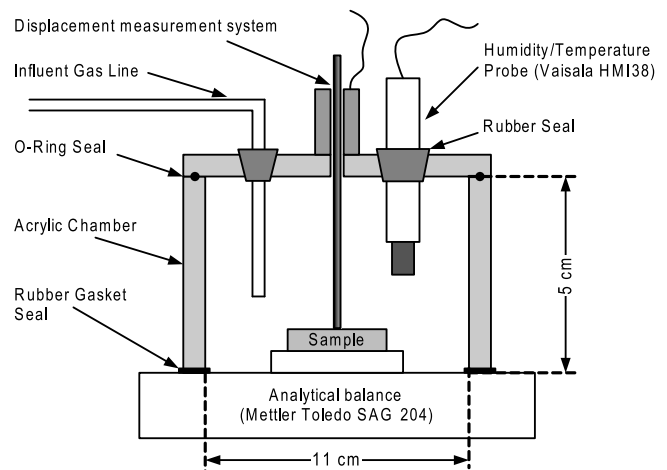


Figure 2. Detail of the automated humidity system of the environmental chamber (modified from *Likos and Lu* [2003]).

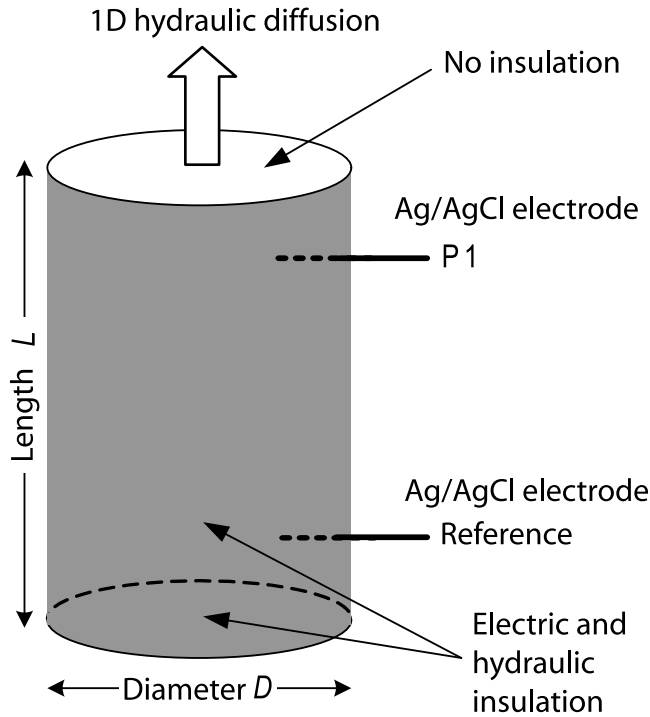


Figure 3. Sketch of the 1-D hydraulic diffusion experiment monitored by the streaming potential method. The streaming potential measurements are performed with the nonpolarizing electrode P1 and the reference electrode. The sample is insulated on the side and below. The loss of the water occurs through the upper face only.

Indeed 30% relative humidity is indicative of extremely dry conditions and fluxes of any kind (films or vapor phase) are extremely low at such low potentials.

[21] 4. Electroosmosis is neglected [see *Revil et al.*, 1999].

[22] 5. Lateral deformations are neglected (1-D assumption) and the stress applied to the sample is equal to the atmospheric pressure (see Appendix A).

[23] According to the model developed by *Olchitzky* [2002] and *Homand et al.* [2004], the relative variation of the mass of the sample from the initial (i) state is given by (see Appendix A)

$$\Theta(\bar{\mathbf{m}}, t) \equiv \frac{\Delta M_w(t)}{M_i} \approx -\frac{\rho_w \Omega}{M_i} (\bar{p}_c^{imp} - \bar{p}_c^i) \eta_i \left[1 - \sum_{n=0}^{\infty} E_n(t) \right], \quad (21)$$

where η_i is the specific storage expressed in Pa^{-1} [*Homand et al.*, 2004], M_i is the initial mass of the sample at time t_i , and $\bar{\mathbf{m}}$ is the vector of model parameters that will be determined by optimization for the initial condition i . The other variables and functions are defined by [*Homand et al.*, 2004]

$$E_n(t) = \frac{8}{(2n+1)^2 \pi^2} \exp \left[-\frac{k_w^{r,i} k}{\eta_w \eta_i} \omega_n^2 t \right], \quad (22)$$

$$\omega_n = \frac{(2n+1)\pi}{L}, \quad (23)$$

$$\Omega = \pi R^2 L, \quad (24)$$

$$\eta_i = \left(\frac{\alpha^2}{\lambda_i + 2G} + N \right) (s_w^i)^2 + \phi_i \left[\frac{s_w^i}{K_w} - \left(\frac{\partial s_w}{\partial p_c} \right)_i \right], \quad (25)$$

where R is the radius of the sample, L is its length (Ω is the volume of the sample), η_i is the specific storage coefficient λ_i is the Lamé modulus in the initial reference state, G is the shear modulus (independent of the saturation), K_w is the bulk modulus of the wetting phase (liquid

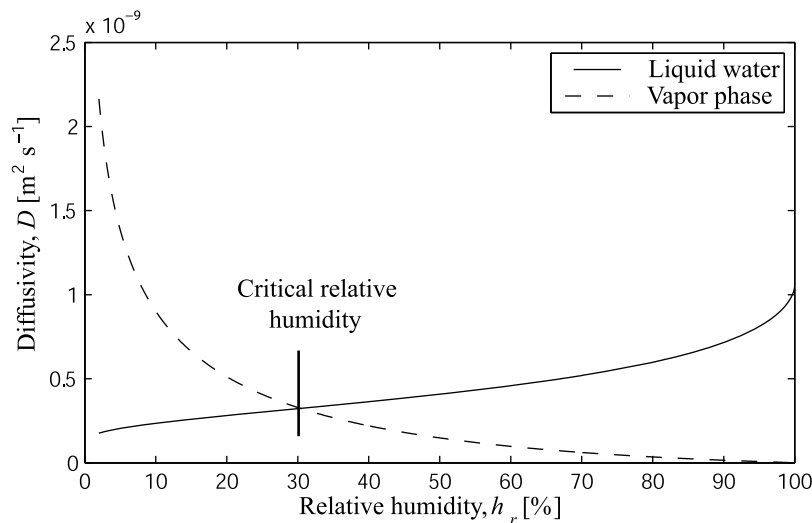


Figure 4. Comparison between the contribution D_v^i and D_w^i of the overall hydraulic diffusivity of water through the clay rock. The contribution D_v^i is related to the hydraulic diffusion of the vapor phase, while the contribution D_w^i is related to the hydraulic diffusion of the liquid water phase. The diffusion of the vapor phase can be neglected above a critical relative humidity of 30%. We used $D_v = 2.5 \times 10^{-5} \text{ m}^2 \text{ s}^{-1}$.

Table 3. Characteristics and Geometrical Properties of the Callovo-Oxfordian Samples Used in the Present Work

Sample	Borehole	Depth (m)	Unit	Length, L (m)	Diameter, D (m)	Experiment
EST28242	EST423	620.83	C2b1	0.010	0.051	HM ^a
EST29296	EST433	617.55	C2b1	0.064	0.065	SP ^b

^aHydromechanical measurements.

^bStreaming potential measurements.

water), α is the classical Biot coefficient, and N is a stiffness coefficient. They are defined by

$$\alpha = 1 - \frac{K}{K_s}, \quad (26)$$

$$N \equiv \frac{(1 - \alpha)(\alpha - \phi)}{K}, \quad (27)$$

where K is the drained bulk modulus and K_s is the bulk modulus of the solid phase [see *Gasc-Barbier*, 2002]. Using this linear approximation, the analysis of the transient streaming potential response during a drying test is provided in Appendix B.

3. Description of the Experiments

[24] Three sets of experiments were performed to study the transport properties of the Callovo-Oxfordian clay rock at different saturations of the water phase. The first experiment was conducted to study the hydromechanical behavior of a single Callovo-Oxfordian clay rock sample under partially saturated conditions to determine its hydromechanical properties (relative permeability and specific storage at different relative water saturations).

[25] The second set of measurements was performed to measure the streaming potential in order to determine the value of the streaming potential coupling coefficient and to see if this approach could be used to monitor the flow of the liquid water during such drying experiments. Finally, a third set of experiments were performed to see how electrical conductivity varies with saturation and to determine Archie second exponent. This Archie second exponent will be related to the exponent used to describe the relative permeability as a function of the saturation in section 5.

3.1. Description of the Core Samples

[26] All the cores used for our experiments were sampled from the Callovo-Oxfordian formation at the Bure test site (Meuse/Haute-Marne, France). The cores were drilled with a NaCl saturated mud (borehole EST423 and EST433) and came as a series of ~20 cm long core cylinders sampled at different depths. The samples from borehole EST433 were resampled to avoid the NaCl contamination on the boundaries. Then all the samples were conditioned in double hermetic bags and confined in polystyrene during their transport from the field to the laboratory.

[27] The samples were already only partially saturated at the beginning of the experiments. Their initial saturation was in the range 0.7 to 0.9. In order to limit hydrochemical disturbances like those associated with a change in the

osmotic pressure, we have decided not to resaturate the samples prior to our experiments. The characteristics of our samples are detailed in Table 3.

3.2. Drying Experiment

[28] The hydromechanical behavior of Callovo-Oxfordian clay rock was studied using the automated humidity system developed by *Likos and Lu* [2001, 2003]. This system is based on the control of the relative humidity of a confined chamber by a general system of air injection. The sample is placed on high-precision analytical balance (Mettler Toledo SAG 204) in a small environmental chamber (5 × 11 cm) that contains a relative humidity–temperature probe (Vaisala HMI38) and a vertical displacement probe (Figures 1 and 2). An influent gas line injects a “humid” gas form in a mixing chamber from a “wet” and a “dry” line. The relative humidity of the gas is adjusted to the humidity measurement in the chamber by two mass flow controllers (Figure 1). Humidity, temperature, mass, and displacements are recorded on a computer at a chosen frequency. Owing to the long duration of the experiments, measurements were taken every 300 s.

[29] The system is able to determine the total suction characteristics of microporous rocks in a relatively high suction range from 7×10^6 Pa to 7×10^9 Pa. During the drying experiment, we monitored the mass variation of the core sample EST28242 for different relative humidity steps in both desaturation ($h_r = 90, 70, 50, 27,$ and 7%) and re-saturation ($h_r = 7, 13, 23, 31, 40, 48,$ and 90%).

[30] The core sample EST28242 (see properties in Table 3) was extracted from the borehole EST423 at depths comprised between 620.73 to 620.93 m. It was reshaped to a smaller cylinder (length of 1 cm and diameter of 5.1 cm) to fit in the apparatus chamber. After the drying-rewetting experiment, the sample was put in an oven to determine the dry mass at 105°C during 24 h. The porosity we considered for our calculations was measured in situ (in the borehole EST423) by TCMR (Total Combinable Magnetic Resonance). It is equal to 0.171.

3.3. Streaming Potential Experiment

[31] Owing to technical constraints, the study of the electrokinetic behavior of a Callovo-Oxfordian clay rock during a drying experiment was done outside the automated humidity system described above. The clay-rock samples were cut to have a cylindrical shape (see Table 3). The bottom and sides of the core samples were impermeable as shown in Figure 3. These evaporation experiments were realized with the following conditions $T = 22 \pm 1^\circ\text{C}$ and $h_r = 20 \pm 2\%$.

[32] For each sample, we used two small nonpolarizable Ag–AgCl electrodes design for medical use (from In Vivo Metric). These electrodes have shown that they provide best lasting without polarization and drifting (more than a couple of weeks in contact to rock and water). They have very small dimensions (0.8 mm thick and 8 mm long), which is ideal for these experiments so the electrical potential measurement can be considered as a point measurement. Two small holes were drilled on the side of the core and filled with a conductive gel (developed for electroencephalography) in order to improve the contact between the electrodes and the clay-rock core sample. The holes were drilled at 1 cm from the cylindrical sample end-faces.

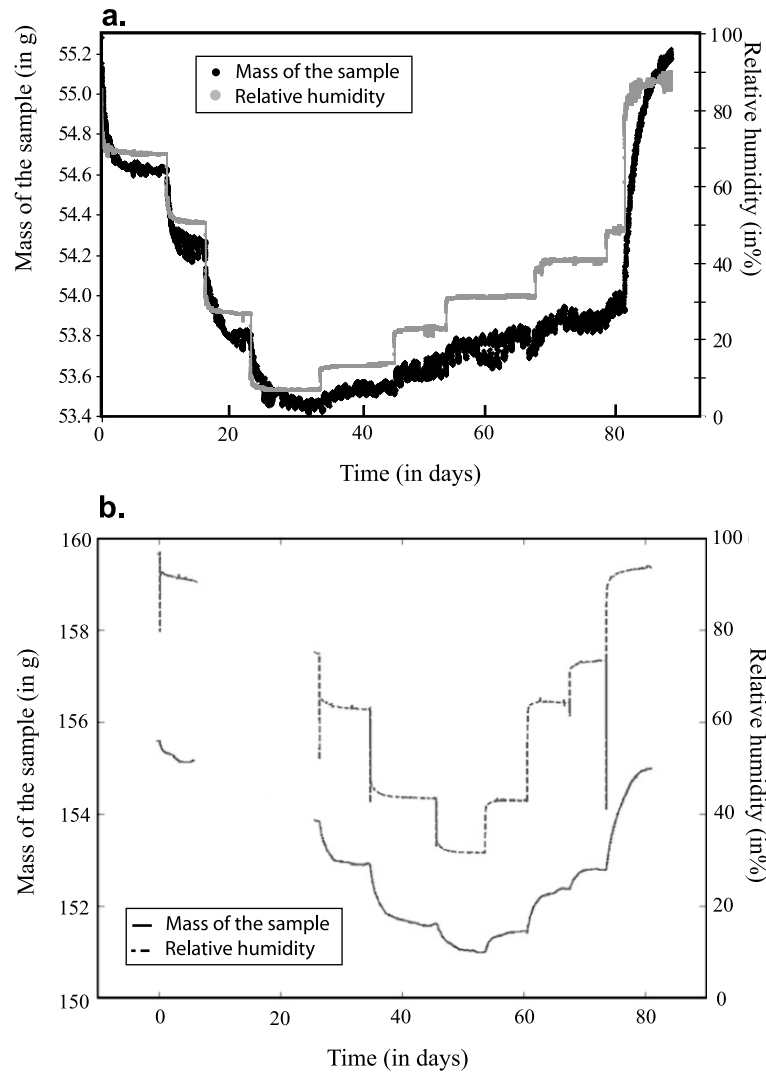


Figure 5. Results from the hydraulic diffusion experiments in an environmental chamber with an automated humidity system. (a) Experimental results from the present study. (b) Results of the experiments conducted by *Pham* [2006] and *Pham et al.* [2007] for comparison.

[33] During the drying tests, the streaming potential resulting from the flow of the water phase was measured by a very precise voltmeter (Fluke 289 Multimeter, sensitivity $\pm 10 \mu\text{V}$) and recorded by a laptop computer. We have also checked the potential drift between the two electrodes before and after the experiment but no drift was observed indicating very stable electrodes. The noise level during the experiments was $\pm 200 \mu\text{V}$.

3.4. Electrical Conductivity Experiments

[34] The electrical conductivity of three core samples was determined from the magnitude of spectral induced polarization measurements in partially saturated conditions following the procedure described by *Cosenza et al.* [2007]. Each sample was dried first at the atmospheric conditions of the laboratory ($T = 22 \pm 1^\circ\text{C}$ and $h_r = 20 \pm 2\%$), then heated 24 h in an oven at three distinct temperatures: 70, 90, and 105°C . The electrical conductivity measurements were made at different saturations using the equipment developed at the Central Laboratory for Electronics (ZEL) at the For-

schungszentrum Jülich, Germany [see *Zimmermann et al.*, 2008]. It is based on a four-electrodes device measuring the conductance of the rock samples in the frequency range 1 mHz to 45 kHz. A complete analysis and modeling of the complex resistivity measurements can be found in *Joungnot et al.* [2010].

4. Interpretation

4.1. Drying Experiment

[35] Sample EST28242 was dried in the automatic system during 34 days (2.92×10^6 s) and then resaturated during 62 days (5.35×10^6 s). Figure 5a presents the raw data of relative humidity and the sample mass as a function of time. Significant temperature changes in the laboratory ($\pm 2^\circ\text{C}$) did not allow us to acquire reliable data for the resaturation. Therefore, we will focus only on the drying experiment below. During the drying procedure, the temperature was relatively stable around 24°C and the displacement probe data did not show any measurable variations in the sample

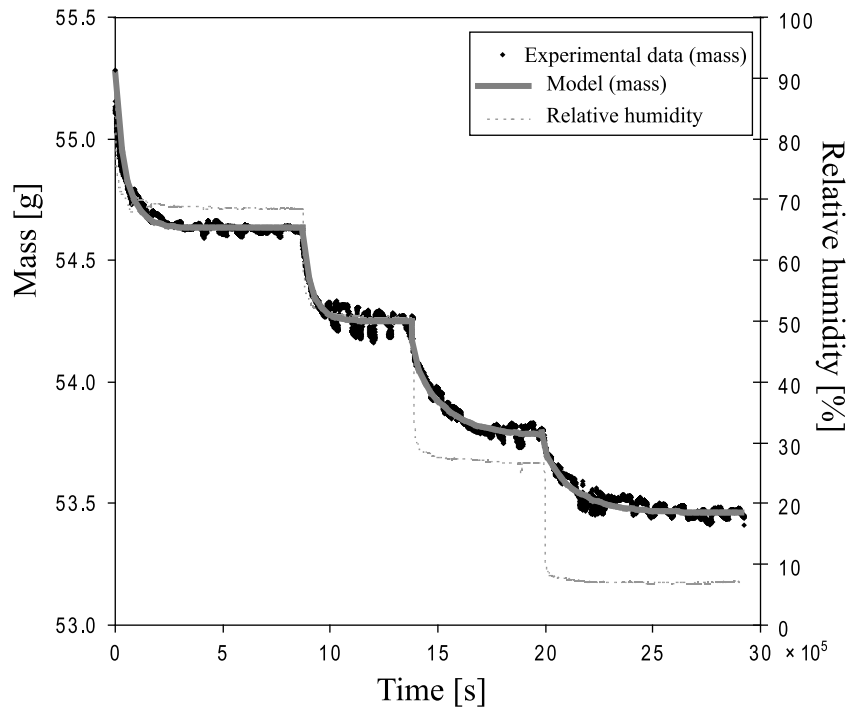


Figure 6. Step by step simulation of the mass variation during the drying experiment by the 1-D approximation of the proposed model. The black dots correspond to the mass of the sample measured by the high-precision balance. The large solid gray line is the model with the model parameters optimized with the Simplex algorithm. The dotted line corresponds to the relative humidity values. There are four initial states considered for this experiment. Its duration is approximately 35 days.

thickness so they are not discussed further in the present paper.

[36] For each equilibrium at an h_r value, it is possible to determine first the capillary pressure and then the relative saturation and therefore to determine the sorption curve. The capillary pressure is determined from Kelvin equation and the recorded values of the relative humidity. The saturations of the samples were monitored through their weight with a precision balance (± 0.0001 g). The sample water saturations are calculated from

$$s_w = \frac{w}{\phi} \frac{\rho_d}{\rho_w}, \quad (28)$$

where $w = (m_{meas} - m_d)/m_d$ is the gravimetric water content with m_{meas} , the measured mass, and m_d , the dry mass of the sample. ϕ is the “Total Combinable Magnetic Resonance” (TCMR) porosity, $\rho_w = 1000 \text{ kg m}^{-3}$, and $\rho_d = (1 - \phi)\rho_g$ are the water and the dry density, respectively (with $\rho_g = 2690 \text{ kg m}^{-3}$ the grain density; see *Gaucher et al.* [2004]).

[37] The Simplex algorithm [*Caceci and Cacheris*, 1984] was applied to the 1-D approximation of the model presented above in section 2, equations (21)–(25), to invert the permeability k_w^i and the specific storage coefficient η_i of sample EST28242 from the drying experiment. No regularization term was added to the data misfit function to perform the optimization because the optimization is well-posed. The inversion was performed at each step in the drying procedure. The subscript “i” stands for the initial state when the determined parameter corresponds, at each step, to the equilibrium condition (capillary pressure, water saturation) before the relative humidity drop was made in

the chamber. The Simplex algorithm was also applied to the data of *Pham* [2006] (see Figure 5b). These experimental data provides additional data points to determine the relative permeability versus the saturation of the liquid water phase.

[38] Considering the core sample EST28242, Figure 6 shows that the analytical solution for the 1-D hydraulic diffusion fits well the experimental data at every drop in the relative humidity during the drying procedure. As expected from the literature data, the permeability $k_w(s_w)$ fitted at different steps decrease with the saturation (Table 4): from $k_w(0.70) = 3.32 \times 10^{-22} \text{ m}^2$ to $k_w(0.23) = 4.01 \times 10^{-24} \text{ m}^2$.

[39] The relative permeability follows a power law function: $k_w^i = s_w^\lambda$ with $\lambda = 4.3 \pm 0.1$ (Figure 7) and the permeability at saturation is given by $k_w(1) = 1.749 \times 10^{-21} \text{ m}^2$. This saturated value of permeability corresponds to the range of values reported in the literature for the Callovo-Oxfordian clay rock $k \in [10^{-22}; 10^{-20}] \text{ m}^2$ [see *Homand et al.*, 2004; *Escoffier et al.*, 2005]. The value of the exponent λ

Table 4. Fitted Hydraulic Parameter for the EST28242 Sample at Different Saturations From the Drying Procedure Experiment

Saturation, s_w^i (-)	Permeability, k_w^i (m^2)	Specific Storage Coefficient, η_i (Pa^{-1})	Root-Mean-Square, RMS (%)
0.69	3.32×10^{-22}	4.85×10^{-10}	0.0284
0.54	1.78×10^{-22}	2.28×10^{-10}	0.0452
0.43	3.61×10^{-23}	1.33×10^{-10}	0.0388
0.33	1.39×10^{-23}	5.00×10^{-11}	0.0357
0.23	4.01×10^{-24}	1.58×10^{-11}	0.0326
1.00 ^a	1.75×10^{-21}	1.66×10^{-9}	NA

^aExtrapolated using the power law behavior between the relative permeability and saturation.

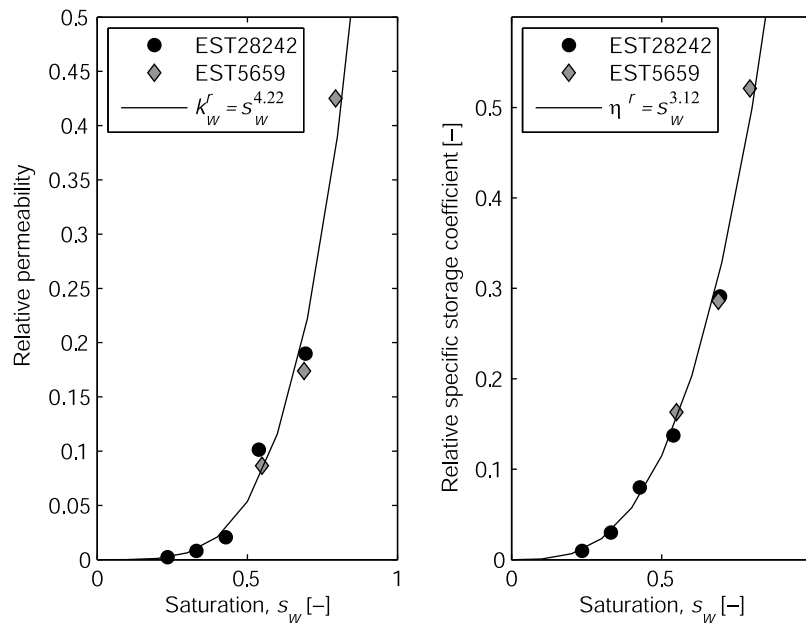


Figure 7. Fitted relative permeability and relative storage coefficient term versus saturation in two Callovo-Oxfordian clay-rock samples: sample EST28242 (black dots, this study) and sample EST5659 (gray diamonds, data from *Pham* [2006]). Samples EST28242 and EST5659 have a porosity of 0.171 and 0.14, respectively. The solid lines correspond to the two best fits obtained by a power law function for the presented data set. The uncertainties are comprised inside the size of the symbols.

can be compared with the value found by *Pham* [2006]: $\lambda = 3.5$ for desaturation and 3.0 for resaturation. We believe that the low value obtained by *Pham* [2006] may be due to the presence of microcracks in their samples. This will be discussed in section 5.

[40] The specific storage coefficient also decreases with the desaturation (Table 4) from $\eta(0.69) = 4.85 \times 10^{-10} \text{ Pa}^{-1}$ to $\eta(0.23) = 1.58 \times 10^{-11} \text{ Pa}^{-1}$. The relative specific storage coefficient with respect to the value at saturation follows a power law relationship $\eta^r = s_w^{3.17}$ (Figure 8). The specific storage at saturation is given by $\eta^s = 1.66 \times 10^{-9} \text{ Pa}^{-1}$. This saturated value is comprised between the value found by *Homand et al.* [2004] ($\eta(0.97) = 1.5 \times 10^{-9} \text{ Pa}^{-1}$) and the value determined by *Giraud et al.* [2007] ($\eta(0.98) = 2.06 \times 10^{-9} \text{ Pa}^{-1}$) in the vicinity of saturation. The specific storage coefficient can also be used to estimate the compressibility of the pores at saturation given by: $\beta_p = \eta^s - \phi\beta_w$ where $\beta_w = 1/K_w$ is the compressibility of the pore water ($4.8 \times 10^{-10} \text{ Pa}^{-1}$) and ϕ is the connected porosity (close to 0.17 in our case). This yields $\beta_p = 1.58 \times 10^{-9} \text{ Pa}^{-1}$, so the pores are highly compressible.

[41] The relative permeability $k_w^{r,i}$ and relative specific storage coefficient η_i^r fitted by the Simplex algorithm from EST28242 data are compared to the values determined by our approach using the raw experimental data of *Pham* [2006] in Figure 7 (sample EST5659, porosity of 0.14). The saturated values for EST5659 were determined along the same procedure than for sample EST28242 (a fitted power law). From these results, it seems that a power law function is able to fit the data, at least on a middle saturation range (from 0.2 to 0.8): $k_w^r = s_w^\lambda$, with $\lambda \approx 4.2$ like in the *Brooks and Corey* [1964] model.

[42] We can also determine the specific storage from the poroelastic properties of the Callovo-Oxfordian clay rock

(Table 1) and the capillary pressure curve. The sorption curve parameters of equation (4) were fitted to sample EST27242 data using the Simplex algorithm. The results are shown in Figure 9. The best fit for sample EST28242 is obtained with $a_{vv} = 228 \text{ m}$ and $b_{vv} = 0.621$ in equation (4).

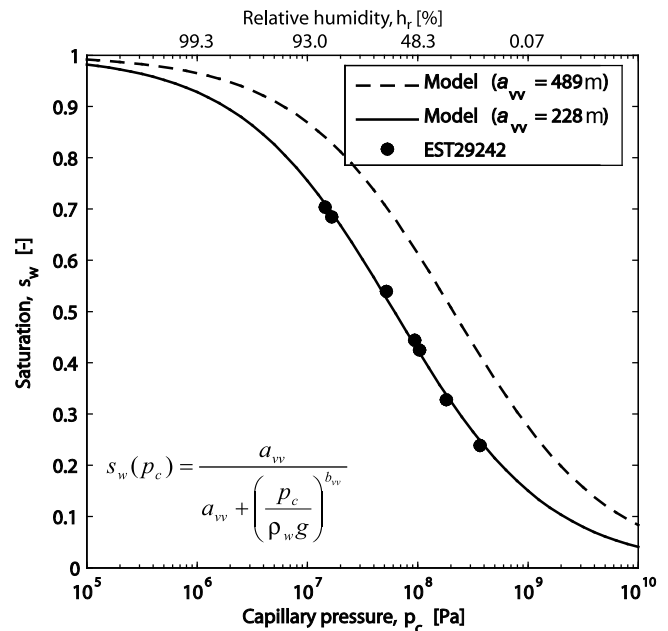


Figure 8. Sorption curve fitted by the Vachaud-Vauclin model (both with $b_{vv} = 0.621$): the solid line represents the best fit for $a_{vv} = 228 \text{ m}$, and the dashed line represents the sorption curve for $a_{vv} = 489 \text{ m}$ (sample EST28242). The uncertainties are comprised inside the size of the symbols.

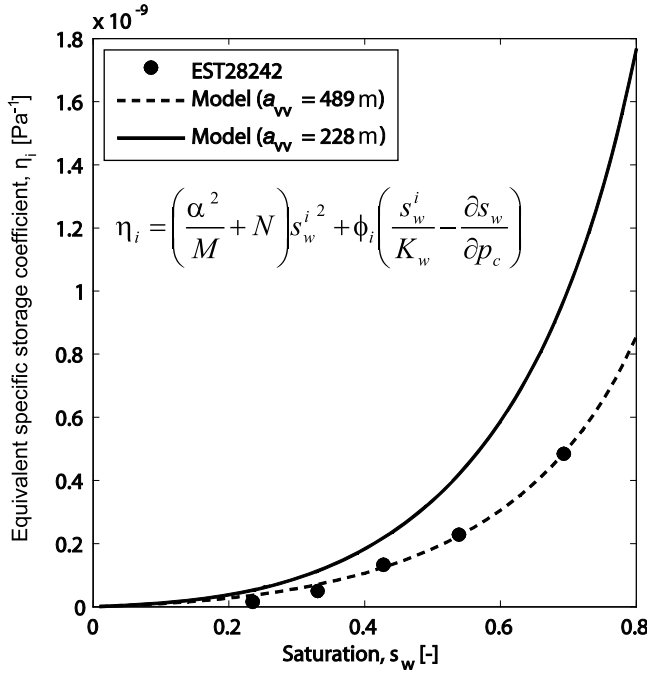


Figure 9. Specific storage coefficient η_i as a function of saturation, determined by the 1-D analytical solution of the proposed model with the sorption curve values ($a_{vv} = 228$ m and $b_{vv} = 0.621$, the solid line) and with the best fit values ($a_{vv} = 489$ m and $b_{vv} = 0.621$, the dashed line). The uncertainties are comprised inside the size of the symbols.

Using these two parameters with the poroelastic properties of the Callovo-Oxfordian clay rock, we calculated the specific storage as a function of saturation (Figure 8). There is a nonnegligible difference between the calculated (Figure 8, solid line) and determined (Figure 8, black dots) specific storages. However, the overall trend is pretty good. Using $a_{vv} = 489$ m (and keeping $b_{vv} = 0.621$), the model (Figure 8, dashed line) fits the data. This difference in the value of a_{vv} can be explained by the uncertainty related to the value of the porosity and therefore on the exact level of saturation.

4.2. Streaming Potential Experiment

[43] The streaming potential experiments were conducted on one sample following the procedure describe in section 3.3. The hydraulic diffusion generates therefore a measurable transient and positive streaming potential signal with the amplitude reaching 25 mV in Figure 10. This observation is consistent with the basic theory described by equation (13). The polarity of the streaming potential is expected to be positive because the excess of charge contained in the pore water is positive and because the recording electrode is downstream and the reference electrode is upstream at the bottom of the core sample. According to equation (13), the peak corresponds to the maximum of the pore water velocity. From the equations presented in Appendix B, it is possible to compute the coupling coefficient at initial condition ($s_w = 0.73$) for sample EST29296 using again the Simplex algorithm. We obtain $C_i = -0.68$ mV m⁻¹. To see if this value is meaningful, we need to compare with a model for the streaming potential coupling coefficient.

[44] The electrokinetic properties of partially saturated porous media were modeled by *Linde et al.* [2007] and *Revil et al.* [2007] using a volume-averaging approach. They derived the following formula to compute the streaming potential coupling coefficient at a given saturation:

$$C(s_w) \equiv - \left(\frac{\partial \varphi}{\partial p_c} \right)_{j=0, T, \bar{p}_n} = - \frac{k_w(s_w)}{\eta_w \sigma(s_w)} \left(\frac{\bar{Q}_Y}{s_w} \right), \quad (29)$$

$$C(s_w) = \frac{k_w^r}{\sigma_r} \left(\frac{1}{s_w} \right) C_{sat}, \quad (30)$$

where C_{sat} is the value of the coupling coefficient at full saturation of the liquid water phase and σ_r is the relative electrical conductivity (the ratio of the conductivity at a given saturation divided by the conductivity at full saturation). *Revil et al.* [2007] showed that equations (29) and (30) reproduce very well the experimental data of *Revil and Cerepi* [2004] for carbonate rocks. We found above that the relative permeability of the water phase is given by $k_w^r \approx s_w^\lambda$. The relative DC-electrical conductivity can be determined using equation (18) without the Stern layer contribution. This yields $\sigma_r \approx s_w^n$. Then equation (30) becomes: $C(s_w) = s_w^{\lambda-n-1} C_{sat}$. Figure 11 shows the simulation of the relative coupling coefficient as a function of saturation and

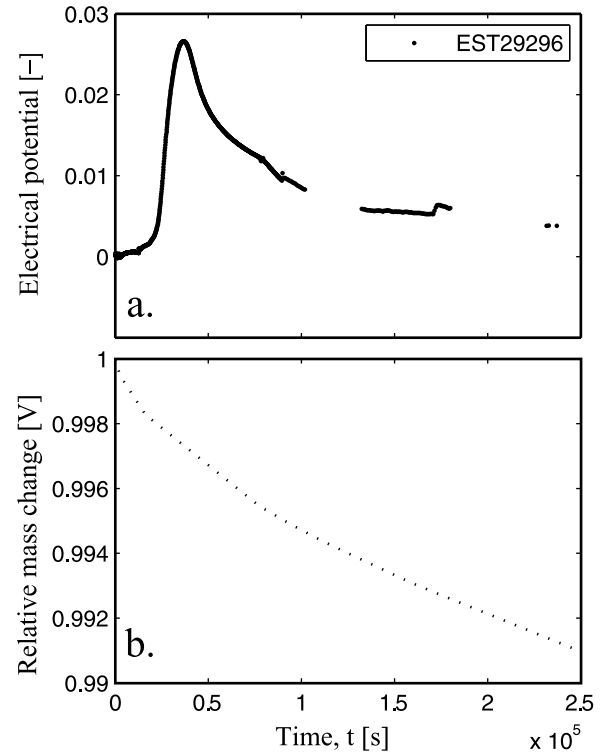


Figure 10. Results of the streaming potential monitoring experiment for sample EST29296. (a) Self-potential versus time (the uncertainty on the measurement is 0.02 mV). (b) Change in the mass of the sample over time. The streaming potential response is sensitive to the flow of the liquid water only while at very low relative humidity (20% here); the loss of water is driven both by the diffusion of vapor and the flow of the liquid water (see Figure 4).

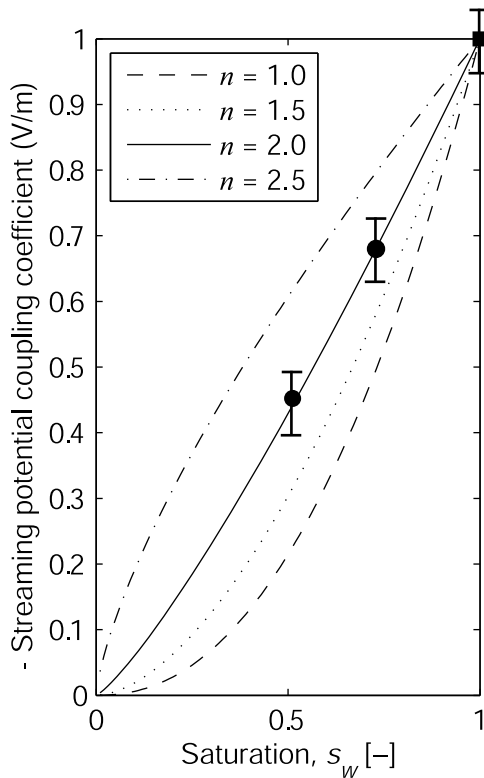


Figure 11. Streaming potential coupling coefficient versus saturation showing the influence of the saturation index n (with $\lambda = 4.22$). The black dots represent the coupling coefficient from sample EST29296, while the black square is the value reported by *Revil et al.* [2005] (at a pore water conductivity $\bar{\sigma}_w = 0.708 \text{ S m}^{-1}$ determined from the composition of the pore water at saturation of the water phase; see Table 2).

the influence of the two exponents λ and n . Considering *Revil et al.* [2005] experimental data, the coupling coefficient of the Callovo-Oxfordian clay rock at saturation (sample EST29296) at the pore water conductivity $\bar{\sigma}_w = 0.708 \text{ S m}^{-1}$ (see section 4.3) is equal to $C_{sat} = -1.0 \text{ mV m}^{-1}$. Figure 11 shows that our model agrees with these experimental data points with $\lambda = 4.22$ and $n = 2.0$.

4.3. Electrical Conductivity Experiments

[45] We consider below the electrical conductivity obtained at 10 Hz for the following samples: EST28144, EST29296, and EST30749 (Figure 12). The conductivity of the pore water is computed as [*Revil and Linde, 2006*]

$$\bar{\sigma}_w = \sum_{i=1}^N |q_i| \beta_i \exp\left[-\frac{q_i \varphi_m}{k_b T}\right], \quad (31)$$

where β_i is the mobility of ion i (in $\text{m}^2 \text{ s}^{-1} \text{ V}^{-1}$), q_i is the charge of species i (in C), k_b is the Boltzmann constant ($1.3807 \times 10^{-23} \text{ J K}^{-1}$), T is the absolute temperature (in K), and φ_m is the mean (microscopic) electrostatic potential (in V) in the pore space of the clay rock because of the

diffuse layer. The pore water chemistry in the pore space of the Callovo-Oxfordian clay rock is taken from the THERMOAR model (see Table 2, *Gaucher et al.* [2006], and *Leroy et al.* [2007]).

[46] The conductivity data reported in Figure 12a were fitted with equations (18) and (31) using the Simplex algorithm. The fits are shown in Figures 12b–12d. The optimized parameters for the electrical conductivity measurements are reported in Table 4. We conclude that the electrical conductivity data are well described by equation (18). Indeed, the second Archie exponent, $n = 2.0 \pm 0.5$, is in agreement with an estimate obtained independently from thermal conductivity data in unsaturated conditions [*Jougnot and Revil, 2010*]. The values of the electrical potential in the pore space φ_m and the formation factors are in agreement with independent estimates determined from the diffusion of ionic tracers for the same material [see *Jougnot et al., 2009, Figure 12*]. Therefore we can conclude that our previous model of electrical conductivity, initially developed to determine the electrical conductivity at full saturation, can be used to determine the effect of the saturation upon the magnitude of the electrical conductivity for the Callovo-Oxfordian clay rock as well.

5. Permeability From Electrical Conductivity

[47] In this section, we test the idea proposed recently by *Doussan and Ruy* [2009] to connect the electrical conductivity at a given saturation with the permeability at the same saturation. This may offer a nonintrusive way to determine the permeability in unsaturated conditions using time lapse electrical resistivity tomography. The semiempirical relationship developed by *Doussan and Ruy* [2009] was successfully tested against laboratory and literature data only on relatively permeable soils. They showed that parameters of this relationship can be completely determined with accessible measurements of saturated permeability, electrical conductivity of the pore water, and clay content. In this section, we check if their relationship applies to the very low permeability clay rocks investigated in the present work.

[48] The relationship between the diameter d (in m) of the largest filled pore in contact with air at the matric potential Ψ and the matric potential (in m) is $d \approx 29 \cdot 10^{-6}/|\Psi|$ at 20°C. Using our conductivity model and adapting the general idea of *Doussan and Ruy* [2009], the permeability is approximately given by

$$k(s_w) = \frac{A s_e^n}{F[\Psi(s_w)]^2}, \text{ as } \frac{A s_e^n}{F[\Psi(s_w)]^2} < k_{sat}, \quad (32)$$

$$k(s_w) = k_{sat}, \text{ as } \frac{A s_e^n}{F[\Psi(s_w)]^2} \geq k_{sat}, \quad (33)$$

where F/s_e^n represents the saturation dependence of electrical conductivity, F is the formation factor, and the parameter A (in m^4) depends mainly on the permeability at saturation as discussed below.

[49] In our model, the capillary pressure–saturation relationship can be obtained from equation (4):

$$\Psi(s_w) \approx \left[\frac{a_{vw}(s_w - 1)}{s_w} \right]^{1/b_{vw}}. \quad (34)$$

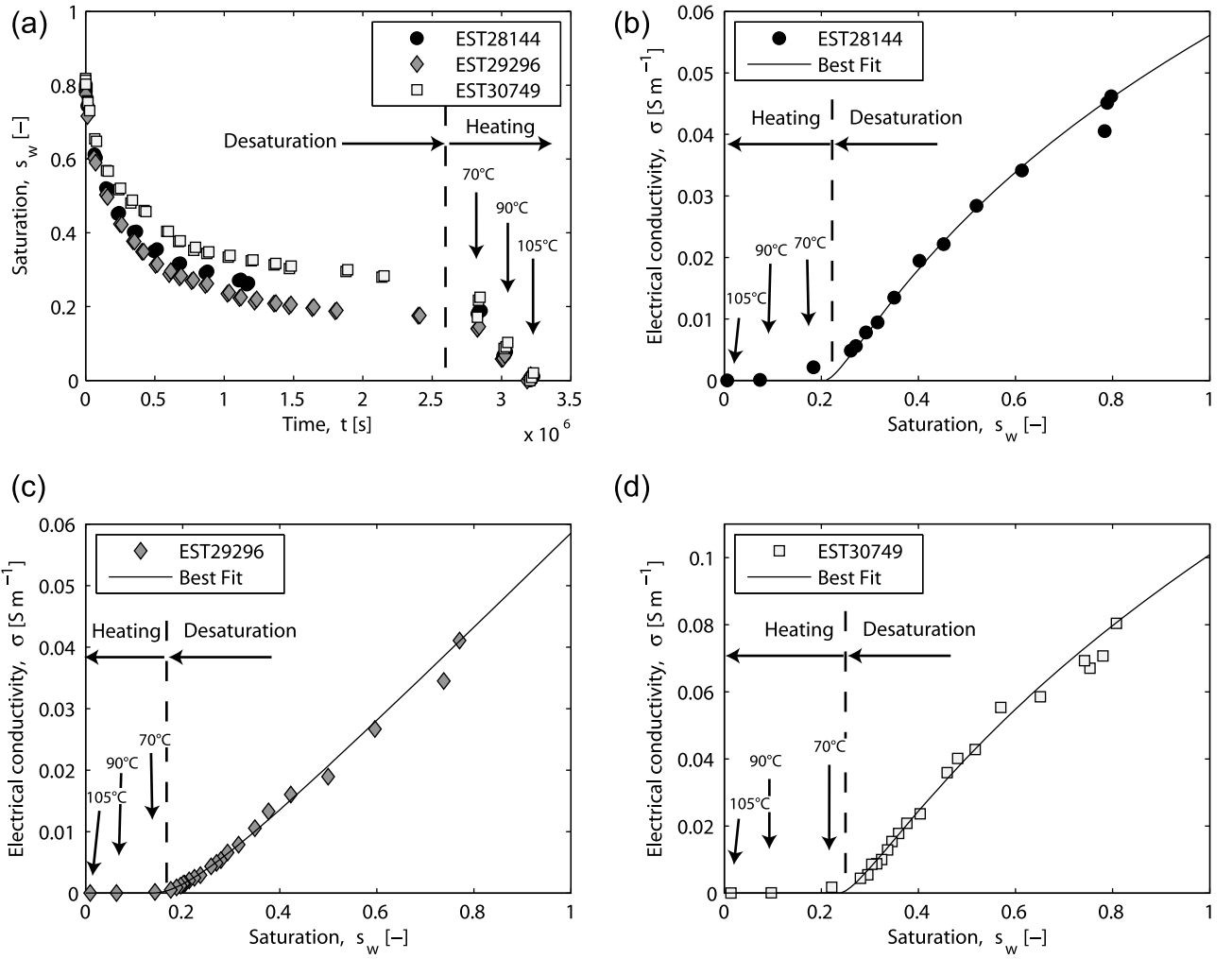


Figure 12. Change in the electrical conductivity during drying for three samples. (a) Saturation of the water phase (calculated from measured mass and given porosities) versus time. (b–d) Electrical conductivity versus saturation. The solid lines correspond to the best fit of the model discussed in the main text.

Combining equations (32) and (34), the permeability can be written as

$$k(s_w) = \frac{A s_w^{n+2/b_{vv}}}{F a_{vv}^{2/b_{vv}} (s_w - 1)^{2/b_{vv}}} \text{ as } \frac{A s_w^{n+2/b_{vv}}}{F a_{vv}^{2/b_{vv}} (s_w - 1)^{2/b_{vv}}} < k_{sat}, \quad (35)$$

$$k(s_w) = k_{sat}, \text{ as } \frac{A s_w^{n+2/b_{vv}}}{F a_{vv}^{2/b_{vv}} (s_w - 1)^{2/b_{vv}}} > k_{sat}. \quad (36)$$

The term $(s_w - 1)^{2/b_{vv}}$ is responsible for a divergence of this expression near saturation. At low saturations, $s_w \ll 1$, we can write

$$k_w^r \approx s_w^{n+2/b_{vv}}, \quad (37)$$

$$k_{sat} = \frac{A}{F a_{vv}^{2/b_{vv}}}, \quad (38)$$

and therefore equation (38) provides a relationship between A and k_{sat} . Using the result found in section 4, $k_w^r = s_w^\lambda$ with $\lambda \approx$

4.2 ± 0.1 and using the electrical conductivity data, we found $\lambda \approx n + 2/b_{vv}$. Using $n = 1.6 \pm 0.2$ (see Table 5) and $b_{vv} = 0.6 \pm 0.2$ (see section 4.1), we obtain $\lambda \approx 4.8 \pm 0.8$ in fair agreement with the value given above ($\lambda \approx 4.2$). In the presence of microcracks, the value of n is lower than for an intact rock sample. For the Callovo-Oxfordian formation, *Joungnot et al.* [2010] found that $n = 1.44$ for a clay-rock sample with microcracks. In this case, using $\lambda \approx n + 2/b_{vv}$ with the $b_{vv} = 1.05$ (see Table 1), we obtain $\lambda = 3.34$. This compares very well with the values found by *Pham* [2006]: $\lambda = 3.5$, which may imply that their sample had microcracks.

[50] Taking $F = 60$ (see Table 5), $a_{vv} = 228$ (see Figure 8), and $k_{sat} = 1.75 \times 10^{-21} m^2$, equation (38) yields $A = 2.4 \times$

Table 5. Fitted Parameters of the *Revil et al.* [2007] Model From the Electrical Conductivity Measurements at 10 Hz

Sample	φ (-)	F (-)	s_w^c (-)	n (-)	φ_m^a (mV)	σ_S ($S m^{-1}$)
EST28144	0.176	80.7	0.21	1.44	-44.5	1.33×10^{-5}
EST29296	0.163	80.0	0.14	1.99	-45.0	0.99×10^{-5}
EST30749	0.181	38.0	0.24	1.50	-42.0	3.25×10^{-5}

^aValue at saturation.

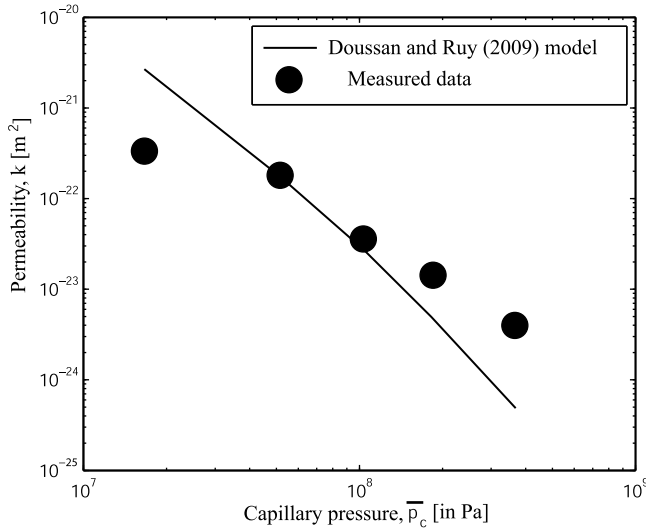


Figure 13. Comparison between our experimental data and the *Doussan and Ruy* [2009] model. We consider $F = 60^\circ$ (mean of the value of the formation factor for the three samples), $n = 1.6$, $s_w^c = 0.1$, $k_s = 1.75 \times 10^{-21} \text{ m}^2$ (permeability at saturation), and $A = 0.91 \times 10^{-12}$ (see equation (39)). The model corresponds to the prediction of equation (32).

10^{-12} m^4 . In the model developed by *Doussan and Ruy* [2009], the following expression of A is obtained by fitting data for various soil samples:

$$A \approx 6.86 \cdot 10^{-4} \left(\frac{k_{sat} \rho_w g}{\eta_w} \right)^{0.645}. \quad (39)$$

Taking $k = 1.75 \times 10^{-21} \text{ m}^2$ (permeability at saturation) yields $A = 0.9 \times 10^{-12} \text{ m}^4$ in fair agreement with the estimate given above. A comparison between our data and the model of *Doussan and Ruy* [2009] is shown in Figure 13. There is a fair comparison between the data and this model. In other words, our data are consistent with the model of *Doussan and Ruy* [2009], and this extends therefore its domain of validity to very low permeability materials. This is an important finding as it means that time-lapse resistivity measurements may be used to assess the change in the relative permeability of such materials characterized by extremely low values of their permeability.

6. Concluding Statements

[51] Determining the saturated properties of very low permeability materials is already a challenging task but, determining their unsaturated properties has been barely performed in the literature with the exception of few recent works at high saturations. In the present paper, we have obtained the relative permeability and specific storage for a wide range of water saturations of very low permeability (sub-nanodarcy) clay rocks. In addition, we have tested the possibility to use the streaming potential method to monitor the flow of the liquid water phase during drying. The interesting property about the streaming potentials, in this context of unsaturated flow with potential transport of water as a

vapor phase, is the fact that these electrical measurements are only sensitive to liquid water phase movement.

[52] We also performed electrical conductivity experiments to see the impact of the saturation upon the electrical conductivity of the Callovo-Oxfordian clay rock and how electrical conductivity can be used to determine relative permeability. We have shown that the dependence of the material properties with saturation can be determined from two exponents only: the first and second Archie exponents. Therefore the present model of the material properties needs only very few input information that can be obtained non-intrusively from two geophysical methods: the self-potential method and electrical resistivity tomography.

Appendix A: 1-D Approximation of the Hydromechanical Problem

[53] In this appendix, we solve the 1-D hydromechanical flow problem corresponding to the drying experiment described in the main text. Because the pressure of the nonwetting phase is constant during the experiment, we will neglect the advective transport of the nonwetting phase in the flux of the vapor phase (see below the boundary conditions). We also neglect the dispersion term in equation (13). This yields

$$\rho_v \dot{\bar{\mathbf{w}}}_v = -\frac{\rho_v}{\bar{p}_v} D_m \nabla \bar{p}_v, \quad (A1)$$

where D_m is the effective diffusion coefficient of the vapor phase through the porous material. Water exists as a liquid and as a vapor phase. The mass conservation of the pore water is therefore expressed as

$$\nabla \cdot (\rho_w \dot{\bar{\mathbf{w}}}_w + \rho_v \dot{\bar{\mathbf{w}}}_v) = -\frac{\partial}{\partial t} (m_w + m_v) + Q_S, \quad (A2)$$

where m_w and m_v represent the mass of liquid water and vapor per unit volume of the porous material and Q_S corresponds to a source or sink term (mass per unit volume per unit time). The source or sink terms will be transferred as a boundary condition at the upper boundary of the sample (see below and *Homand et al.* [2004]). Neglecting the electroosmotic coupling term for the flux of the liquid water phase, we have

$$\rho_w \dot{\bar{\mathbf{w}}}_w = -\frac{\rho_w k_w^r k}{\eta_w} \nabla \bar{p}_w. \quad (A3)$$

Considering the pressure of the nonwetting phase is constant, we have [*Coussy*, 2004]

$$\frac{dm_w}{\rho_w} = \alpha_w d\varepsilon + N_{ww} d\bar{p}_w, \quad (A4)$$

$$N_{ww} = \frac{\phi s_w}{K_w} - \phi \frac{\partial s_w}{\partial p_c} + N_s^2, \quad (A5)$$

where α is the classical Biot coefficient ε represents the bulk deformation of the material, and N is a stiffness coefficient. Using a linearization of the capillary pressure curve, we have [*Homand et al.*, 2004]

$$\frac{\delta m_w}{\rho_w} = \alpha s_w^i d\varepsilon + \left[\phi \left(\frac{s_w^i}{K_w} - \frac{\partial s_w}{\partial p_c} \right) + N_s^{i,2} \right] \delta \bar{p}_w. \quad (A6)$$

The subscript i means that the property is evaluated at the initial condition of the increment in the change of fluid pressure. In addition, for the 1-D consolidation problem, the change in the bulk deformation ε [Homand *et al.*, 2004] is

$$\delta\varepsilon = \frac{\alpha s_w^i}{\lambda_i + 2G} \delta\bar{p}_w, \quad (\text{A7})$$

where λ_i and G are the Lamé coefficients, G is the shear modulus of the material, and λ_i is evaluated at the initial condition of the increment in the change of fluid pressure. Consequently, a small change in the liquid water mass is related to a small change of the effective liquid water pressure by

$$\frac{\delta m_w}{\rho_w} = \eta_i \delta\bar{p}_w, \quad (\text{A8})$$

$$\eta_i = \left(\frac{\alpha^2}{\lambda_i + 2G} + N \right) (s_w^i)^2 + \phi_i \left[\frac{s_w^i}{K_w} - \left(\frac{\partial s_w}{\partial \bar{p}_c} \right)_i \right], \quad (\text{A9})$$

where η_i is the specific storage coefficient. Inserting equation (A8) into equation (A3), we obtain

$$\rho_w \dot{\bar{\mathbf{w}}}_w = - \frac{k_w^r k}{\eta_w \eta} \nabla m_w, \quad (\text{A10})$$

$$\rho_v \dot{\bar{\mathbf{w}}}_v = - \frac{1}{\bar{p}_v \eta} \left(\frac{\rho_v}{\rho_w} \right)^2 D_m \nabla m_w, \quad (\text{A11})$$

where we have used the following relationship:

$$\nabla \bar{p}_v = \frac{\rho_v}{\rho_w} \nabla \bar{p}_w, \quad (\text{A12})$$

determined from the law for perfect gases. Inserting equations (A10) and (A11) into equation (A2) and neglecting $\partial m_v / \partial t$ with respect to $\partial m_w / \partial t$, we obtain the following linearized diffusion equation for the mass of the pore water for each humidity step:

$$\nabla^2 m_w - \frac{1}{D_e^i} \frac{\partial m_w}{\partial t} = 0, \quad (\text{A13})$$

$$D_e^i = \frac{1}{\eta} \left[\frac{k_w^r k}{\eta_w} + \frac{1}{\bar{p}_v} \left(\frac{\rho_v}{\rho_w} \right)^2 D_m \right], \quad (\text{A14})$$

where D_e^i is the linearized diffusion coefficient (in $\text{m}^2 \text{s}^{-1}$). This diffusion coefficient can be written in terms of two contributions:

$$D_e^i = D_v^i + D_w^i, \quad (\text{A15})$$

$$D_w^i = \frac{1}{\eta} \frac{k_w^r k}{\eta_w}, \quad (\text{A16})$$

$$D_v^i = \frac{1}{\eta} \frac{1}{\bar{p}_v} \left(\frac{\rho_v}{\rho_w} \right)^2 D_m. \quad (\text{A17})$$

The contribution D_v^i is related to the hydraulic diffusion for the vapor phase and the contribution D_w^i is related to the hydraulic diffusion of the liquid water. We can evaluate for which conditions the diffusion of the vapor phase can be

neglected. We define the ratio of the two diffusion coefficients as

$$\chi \equiv \frac{D_v^i}{D_w^i} = \frac{\eta_w}{\bar{p}_v k_w^r k} \left(\frac{\rho_v}{\rho_w} \right)^2 D_m. \quad (\text{A18})$$

Using $\rho_v = \bar{p}_v M_v / RT$ with $M_v = 1.8 \times 10^{-2} \text{ kg Mol}^{-1}$, $\bar{p}_v = 0.02 \bar{p}_{atm} = 2 \times 10^3 \text{ Pa}$, $\eta_w = 10^{-3} \text{ Pa s}$, $D_v = 2.5 \times 10^{-5} \text{ m}^2 \text{ s}^{-1}$, $\rho_w = 10^3 \text{ kg m}^{-3}$, and the permeability power law model developed in the main text, we find that the critical relative humidity at which the $\chi = 1$ is 30% (see Figure 4). For relative humidity that are smaller than this value, the measured permeability is an apparent permeability defined by

$$k_a = k_w^r k + \frac{\eta_w}{\bar{p}_v} \left(\frac{\rho_v}{\rho_w} \right)^2 D_m. \quad (\text{A19})$$

Note that the value of the critical relative humidity appears to be sensitive to the assumed form of relative permeability (see the power law function mentioned in the main text).

[54] By integrating the volumetric liquid mass content over the volume of the sample, we obtain the total liquid mass variation:

$$\Delta M_w(t) = 2\pi R^2 \int_0^L (m_w(z, t) - m_w^i) dz. \quad (\text{A20})$$

We denote $\partial\Omega_u$, $\partial\Omega_s$, and $\partial\Omega_b$ as the upper, side, and bottom boundaries of a cylindrical core sample vertically oriented (with axial coordinate z). We denote R and L as the radius and the length of the sample. The boundary conditions for our problem are

$$\hat{\mathbf{n}} \cdot \dot{\bar{\mathbf{w}}}_w = 0, \text{ on } \partial\Omega_s \text{ and } \partial\Omega_b, \quad (\text{A21})$$

$$\bar{p}_c(z, t = t_i) = - \frac{\rho_w RT}{M_v^i} \ln h_r^i, \quad (\text{A22})$$

$$\bar{p}_n(z, t = t_i) = p_{atm}, \quad (\text{A23})$$

$$\bar{p}_v(z, t = t_i) = \bar{p}_v^{sat} h_r^i, \quad (\text{A24})$$

$$\bar{p}_c(z = L, t = t_i^+) = - \frac{\rho_w RT}{M_v^i} \ln h_r^{imp}, \quad (\text{A25})$$

$$\bar{p}_n(z = L, t = t_i^+) = p_{atm}, \quad (\text{A26})$$

$$\bar{p}_v(z, t = t_i) = \bar{p}_v^{sat} h_r^{imp}, \quad (\text{A27})$$

$$\sigma_n(t) = -p_{atm}, \text{ on } \partial\Omega_u, \partial\Omega_s, \text{ and } \partial\Omega_b, \quad (\text{A28})$$

where $\hat{\mathbf{n}}$ is the outward unit vector to the surface of the sample, $z = 0$ corresponds to the bottom of the sample, $z = L$ corresponds to the top boundary, h_r^{imp} is the imposed humidity, and t_i corresponds to the time at which the saline solution is changed, and therefore a new relative humidity h_r^{imp} is imposed at the top boundary of the sample. The

solution for the uniaxial problem described in the main text is given by using the solution of the diffusion equation found in the work of Crank [1975] [see Homand *et al.*, 2004]. This yields

$$\frac{\Delta M_w(t)}{M_i} \approx -\frac{\rho_w \Omega}{M_i} (\bar{p}_c^{imp} - \bar{p}_c^i) \eta_i \cdot \left[1 - \sum_{n=0}^{\infty} \frac{8}{\pi^2 (2n+1)^2} \exp\left(-\frac{D_e (2n+1)^2 \pi^2}{L^2} t\right) \right], \quad (\text{A29})$$

where Ω is the volume of the sample and L is the length of the sample and where we have used the following relationship derived from equation (A8) assuming $d\bar{p}_c = d\bar{p}_n - d\bar{p}_w \approx -d\bar{p}_w$:

$$\Delta m_w \approx -\rho_w \eta_i \Omega (\bar{p}_c^{imp} - \bar{p}_c^i). \quad (\text{A30})$$

Appendix B: Resolution of the Streaming Potential Problem

[55] For one-dimensional flow in a homogeneous core sample, the electrical streaming potential is given by

$$\delta\varphi(z, t) \approx -C [\bar{p}_c(z, t) - \bar{p}_c^i], \quad (\text{B1})$$

where C is the streaming potential coupling coefficient expressing the sensitivity of the electrical field to the gradient of the pore fluid pressure. Using the expression for the capillary pressure as a function of time, we obtain

$$\delta\varphi(z, t) \approx -C (\bar{p}_c^{imp} - \bar{p}_c^i) \left[1 - \sum_{n=0}^{\infty} Y_n(z, t) \right], \quad (\text{B2})$$

where the function $Y_n(z, t)$ is defined by

$$Y_n(z, t) = \frac{4(-1)^{n+1}}{(2n+1)\pi} \cos(\omega_n z) \exp(-\eta_i \omega_n^2 t), \quad (\text{B3})$$

$$\omega_n = \frac{(2n+1)\pi}{L}. \quad (\text{B4})$$

Equation (B2) provides a simple analytical equation to determine the coupling coefficient from the amplitude of the self-potential anomaly.

[56] **Acknowledgments.** We thank the French National Agency for Radioactive Waste Management (ANDRA) (S. Altmann and D. Coelho) for their support. The Ph.D. thesis of Damien Jougnot is supported by ANDRA. The financial support to N. Lu provided by NSF (NSF CMMI-0926276) is appreciated. We thank M. Batzle and A. Jardani for fruitful discussions and T. Young for his support at CSM. We thank the Associate Editor, Tetsu Tokunaga, and three anonymous referees for their constructive comments.

References

Archie, G. E. (1942), The electrical resistivity as an aid in determining some reservoir characteristics, *Trans. Am. Inst. Min. Metall. Pet. Eng.*, *146*, 54–62.

Brooks, R. H., and A. T. Corey (1964), Hydraulic properties of porous media, *Hydrol. Pap. 3*, Colo. State Univ., Fort Collins.

Caccci, M., and W. P. Cacheris (1984), Fitting curves to data: The simplex algorithm is the answer, *Byte*, *9*, 340–362.

Cosenza, P., A. Ghorbani, N. Florsch, and A. Revil (2007), Effects of drying on the low-frequency electrical properties of Tourmemire argillites, *Pure Appl. Geophys.*, *164*, 2043–2066, doi:10.1007/s00024-007-0253-0.

Coussy, O. (2004), *Poromechanics*, 450 pp., John Wiley, New York.

Crank, J. (1975), *The Mathematics of Diffusion*, Clarendon, Oxford, U.K.

Crespy, A., A. Revil, N. Linde, S. Byrdina, A. Jardani, A. Bolève, and P. Henry (2008), Detection and localization of hydromechanical disturbances in a sandbox using the self-potential method, *J. Geophys. Res.*, *113*, B01205, doi:10.1029/2007JB005042.

Croisé, J., L. Schlickerieder, P. Marschall, J. Boisson, P. Vogel, and S. Yamamoto (2004), Hydrogeological investigations in a low permeability claystone formation: The Mont Terri Rock Laboratory, *Phys. Chem. Earth*, *29*, 3–15.

de la Cruz, V., P. N. Sahay, and T. J. T. Spanos (1993), Thermodynamics of porous media, *Proc. R. Soc. London, Ser. A*, *443*, 247–255, doi:10.1098/rspa.1993.0143.

de Vries, D. (1987), The theory of heat and moisture transfer in porous media revisited, *Int. J. Heat Mass Transfer*, *30*(7), 1343–1350, doi:10.1016/0017-9310(87)90166-9.

de Vries, D. A., and A. J. Kruger (1966), On the value of the diffusion coefficient of water in air, *Proc. Colloq. Int. CNRS*, *160*, 61–72.

Doussan, C., and S. Ruy (2009), Prediction of unsaturated soil hydraulic conductivity with electrical conductivity, *Water Resour. Res.*, *45*, W10408, doi:10.1029/2008WR007309.

Escoffier, S., F. Homand, A. Giraud, N. Hoteit, and K. Su (2005), Under stress permeability determination of the Meuse/Haute-Marne mudstone, *Eng. Geol. Amsterdam*, *81*(3), 329–340, doi:10.1016/j.enggeo.2005.06.020.

Gasc-Barbier, M. (2002), Etude des mécanismes de déformation de roches argileuses profondes: Apport de la microstructure et des analyses pétrophysiques, Ph.D. thesis, Univ. Paris VI, Paris.

Gaucher, E., C. Robelin, J. M. Matray, G. Negrel, Y. Gros, J. F. Heitz, A. Vinsot, H. Rebours, A. Cassabagnere, and A. Bouchet (2004), ANDRA underground research laboratory: Interpretation of the mineralogical and geochemical data acquired in the Callovo-Oxfordian Formation by investigative drilling, *Phys. Chem. Earth*, *29*, 55–77.

Gaucher, E., et al. (2006), Modeling the pore water chemistry of the Callovo-Oxfordian formation at a regional scale, *C. R. Geosci.*, *338*(12–13), 917–930.

Gautschi, A. (2001), Hydrogeology of a fractured shale Opalinus clay: Implications for deep geological disposal of radioactive wastes, *Hydrogeol. J.*, *9*, 97–107, doi:10.1007/s100400000117.

Gawin, D., P. Baggio, and B. A. Schrefler (1995), Coupled heat, water and gas flow in deformable porous media, *Int. J. Numer. Methods Fluids*, *20*, 969–987, doi:10.1002/flid.1650200817.

Giraud, A., R. Giot, F. Homand, and A. Koriche (2007), Permeability identification of a weakly permeable partially saturated porous rock, *Transp. Porous Media*, *69*(2), 259–280, doi:10.1007/s11242-006-9073-4.

Giraud, A., R. Giot, and F. Homand (2009), Poromechanical modelling and inverse approach of drying tests on weakly permeable porous rocks, *Transp. Porous Media*, *76*(1), 45–66, doi:10.1007/s11242-008-9229-5.

Homand, F., A. Giraud, S. Escoffier, A. Koriche, and D. Hoxha (2004), Permeability determination of a deep argillite in saturated and partially saturated conditions, *Int. J. Heat Mass Transfer*, *47*(14–16), 3517–3531, doi:10.1016/j.ijheatmasstransfer.2004.02.012.

Jardani, A., A. Revil, W. Barrash, A. Crespy, E. Rizzo, S. Straface, M. Cardiff, B. Malama, C. Miller, and T. Johnson (2009), Reconstruction of the water table from self potential data: A Bayesian approach, *Ground Water*, *47*(2), 213–227, doi:10.1111/j.1745-6584.2008.00513.x.

Jougnot, D., and A. Revil (2010), Thermal conductivity of unsaturated clay-rocks, *Hydrol. Earth Syst. Sci.*, *14*, 91–98, doi:10.5194/hess-14-91-2010.

Jougnot, D., A. Revil, and P. Leroy (2009), Diffusion of ionic tracers in the Callovo-Oxfordian clay-rock using the Donnan equilibrium model and the electrical formation factor, *Geochim. Cosmochim. Acta*, *73*, 2712–2726, doi:10.1016/j.gca.2009.01.035.

Jougnot, D., A. Ghorbani, A. Revil, P. Leroy, and P. Cosenza (2010), Spectral induced polarization of partially saturated clay-rocks: A mechanistic approach, *Geophys. J. Int.*, *180*(1), 210–224, doi:10.1111/j.1365-246X.2009.04426.x.

Leroy, P., and A. Revil (2009), A mechanistic model for the spectral induced polarization of clay materials, *J. Geophys. Res.*, *114*, B10202, doi:10.1029/2008JB006114.

Leroy, P., A. Revil, S. Altmann, and C. Tournassat (2007), Modeling the composition of the pore water in a clay-rock geological formation (Callovo-Oxfordian, France), *Geochim. Cosmochim. Acta*, *71*, 1087–1097, doi:10.1016/j.gca.2006.11.009.

- Leroy, P., A. Revil, A. Kemna, P. Cosenza, and A. Gorbani (2008), Spectral induced polarization of water-saturated packs of glass beads, *J. Colloid Interface Sci.*, *321*(1), 103–117, doi:10.1016/j.jcis.2007.12.031.
- Likos, W. J., and N. Lu (2001), Automated measurement of total suction characteristics in high-suction range: Application to assessment of swelling potential, *Transp. Res. Rec.*, *1755*, 119–128, doi:10.3141/1755-13.
- Likos, W. J., and N. Lu (2003), Automated humidity system for measuring total suction characteristics of clay, *Geotech. Test. J.*, *26*, 179–190.
- Linde, N., D. Jougnot, A. Revil, S. K. Matthäi, T. Arora, D. Renard, and C. Doussan (2007), Streaming current generation in two-phase flow conditions, *Geophys. Res. Lett.*, *34*, L03306, doi:10.1029/2006GL028878.
- Lo, W.-C., G. Sposito, and E. Majer (2002), Immiscible two-phase fluid flows in deformable porous media, *Adv. Water Resour.*, *25*, 1105–1117, doi:10.1016/S0309-1708(02)00050-7.
- Malama, B., A. Revil, and K. L. Kullman (2009), A semi-analytical solution for transient streaming potentials associated with confined aquifer pumping tests, *Geophys. J. Int.*, *176*(3), 1007–1016, doi:10.1111/j.1365-246X.2008.04014.x.
- Olchitzky, E. (2002), Couplage hydromécanique et perméabilité d'une argile gonflante non saturée sous sollicitations hydriques et thermiques courbe de sorption et perméabilité à l'eau, Ph.D. thesis, Ecole des Ponts ParisTech, Paris.
- Pham, Q. T. (2006), Effets de la désaturation et de la resaturation sur l'argilite dans les ouvrages souterrains, Ph.D. thesis, Ecole Polytechnique/X, Paris.
- Pham, Q. T., F. Vales, L. Malinsky, D. Nguyen Minh, and H. Gharbi (2007), Effects of desaturation-resaturation on mudstone, *Phys. Chem. Earth*, *32*, 646–655.
- Revil, A. (2007), Thermodynamics of transport of ions and water in charged and deformable porous media, *J. Colloid Interface Sci.*, *307*(1), 254–264, doi:10.1016/j.jcis.2006.10.074.
- Revil, A., and A. Cerepi (2004), Streaming potential in two-phase flow condition, *Geophys. Res. Lett.*, *31*, L11605, doi:10.1029/2004GL020140.
- Revil, A., and N. Linde (2006), Chémico-electromécanical coupling in microporous media, *J. Colloid Interface Sci.*, *302*, 682–694.
- Revil, A., and P. A. Pezard (1998), Streaming potential anomaly along faults in geothermal areas, *Geophys. Res. Lett.*, *25*(16), 3197–3200, doi:10.1029/98GL02384.
- Revil, A., L. M. Cathles, J. Shosa, P. A. Pezard, and F. D. de Larouziere (1998), Capillary sealing in sedimentary basins: A clear field example, *Geophys. Res. Lett.*, *25*(3), 389–392, doi:10.1029/97GL03775.
- Revil, A., H. Schwaeger, L. M. Cathles, and P. Manhardt (1999), Streaming potential in porous media: 2. Theory and application to geothermal systems, *J. Geophys. Res.*, *104*(B9), 20,033–20,048, doi:10.1029/1999JB900090.
- Revil, A., D. Hermitte, E. Spangenberg, and J. J. Cochémé (2002), Electrical properties of zeolitized volcanoclastic materials, *J. Geophys. Res.*, *107*(B8), 2168, doi:10.1029/2001JB000599.
- Revil, A., V. Naudet, J. Nouzaret, and M. Pessel (2003), Principles of electrography applied to self-potential electrokinetic sources and hydrogeological applications, *Water Resour. Res.*, *39*(5), 1114, doi:10.1029/2001WR000916.
- Revil, A., P. Leroy, and K. Titov (2005), Characterization of transport properties of argillaceous sediments: Application to the Callovo-Oxfordian Argillite, *J. Geophys. Res.*, *110*, B06202, doi:10.1029/2004JB003442.
- Revil, A., N. Linde, A. Cerepi, D. Jougnot, S. Matthäi, and S. Finsterle (2007), Electrokinetic coupling in unsaturated porous media, *J. Colloid Interface Sci.*, *313*(1), 315–327, doi:10.1016/j.jcis.2007.03.037.
- Revil, A., C. Gevaudan, N. Lu, and A. Maineult (2008), Hysteresis of the self-potential response associated with harmonic pumping tests, *Geophys. Res. Lett.*, *35*, L16402, doi:10.1029/2008GL035025.
- Sposito, G. (1981), *The Thermodynamics of Soil Solutions*, Oxford at the Clarendon Press, London.
- Vales, F., D. Nguyen Minh, H. Gharbi, and A. Rejeb (2004), Experimental study of the influence of the degree of saturation on physical and mechanical properties in Tournemire shale (France), *Appl. Clay Sci.*, *26*, 197–207, doi:10.1016/j.clay.2003.12.032.
- Vauclin, M., D. Khanji, and G. Vachaud (1979), Experimental and numerical study of a transient, two-dimensional unsaturated-saturated water table recharge problem, *Water Resour. Res.*, *15*(5), 1089–1101, doi:10.1029/WR015i005p01089.
- Zimmermann, E., A. Kemna, J. Berwix, W. Glaas, H. M. Münch, and J. A. Huisman (2008), A high-accuracy impedance spectrometer for measuring sediments with low polarizability, *Meas. Sci. Technol.*, *19*, 105603, doi:10.1088/0957-0233/19/10/105603.

D. Jougnot and A. Revil, Department of Geophysics, Green Center, Colorado School of Mines, 1500 Illinois St., Golden, CO 80401, USA. (damien.jougnot@unil.ch; arevil@mines.edu)

N. Lu and A. Wayllace, Division of Engineering, Colorado School of Mines, Golden, CO 80401, USA. (ninglu@mines.edu; awayllac@mines.edu)